PCCP

Accepted Manuscript

ROYAL SOCIETY OF CHEMISTRY

rsc.li/pccp

ROYAL SOCIETY OF CHEMISTRY View Article Online
DOI: 10.1039/C8CP02774A

Physical Chemistry Chemical Physics

ARTICAL

Visible-light driven CO_2 photoreduction over $Zn_xCd_{1-x}S$ solid solution coupling with tetra(4-carboxyphenyl)porphyrin iron(III) chloride

Received 00th January 20xx,
Accepted 00th January 20xx

DOI: 10.1039/x0xx00000x

www.rsc.org/

Pan Li,[a,c] Xuehua Zhang,*[a] Chunchao Hou,[b] Lin Lin,[a] Yong Chen*[b,c] and Tao He*[a,c]

Construction of solid solution semiconductor has attracted much attention in photocatalysis by virtue of the tunable elemental composition and band structure. The integration of semiconductor sensitizers with molecular catalysts provides a promising way to fabricate highly efficient, selective and stable system for CO_2 photoreduction. Here $Zn_xCd_{1-x}S$ (ZCS) solid solutions with well-defined floccule-like morphology comprised of nanoribbons are synthesized and used as the photosensitizer to couple with tetra(4-carboxyphenyl)porphyrin iron(III) chloride (FeTCPP) for CO_2 reduction. The effects of changes in surface atom of the ZCS solid solution on the performance of CO_2 photoreduction are investigated. Regardless of the presence of FeTCPP, our results show that introduction of Zn into CdS can affect the activity and selectivity of CO_2 photoreduction, as well as stability of the obtained photocatalysts. More important, the presence of Zn can build efficient electron transfer channels from ZCS to FeTCPP and, thus, greatly facilitating the interfacial charge transfer. Benefitting from the efficient charge separation and electron transfer, ZCS-1/FeTCPP ($Zn_{0.14}Cd_{0.84}S$/FeTCPP) exhibits the highest activity for CO_2 reduction under visible-light irradiation, with CO yield of 1.28 μmol and selectivity up to 93% after 4 h.

Introduction

Inspired by natural photosynthesis, photocatalytic reduction of CO_2 into solar fuels is regarded as a promising solution to supply renewable energy and mitigate carbon emission.[1-6] Molecular catalysts with multiple and accessible redox states can facilitate multi-electron transfer process, and thus have been widely used for CO_2 photoreduction due to their excellent activity and selectivity.[7,8] However, the stability of molecular catalysts is a major obstacle to develop highly efficient photocatalytic systems. Considering inorganic semiconductors usually show superior stability and strong light-absorption ability, semiconductor/molecular catalyst heterogeneous hybrid systems combining the strengths of molecular catalyst and inorganic semiconductor can provide a promising solution to construct highly efficient, selective and stable systems to mimic natural photosynthesis.[1,9-14] In such a hybrid system, the semiconductor acts as light-harvesting antenna and molecular catalyst works as the catalytic center, in which the strong light-harvesting ability and effective interfacial electrons transfer are essential. Hence, modulation of the band structure (conductor/valence band positions and band gap value) of the semiconductor sensitizer and interaction between the semiconductor sensitizer and molecular catalyst are very critical for achieving highly efficient semiconductor/molecular catalyst hybrid photocatalytic systems.[11-14]

Construction of $Zn_xCd_{1-x}S$ (ZCS) solid solution has attracted extensive attention in the field of photocatalysis by virtue of continuously adjustable band structure.[15-17] More importantly, introduction of Zn can tune the structure of surface atoms in CdS, which will affect the adsorption/desorption of the reactants, intermediates, products, and even the hybrid interaction with molecular catalyst and, thereby, have great impact on the photocatalytic activity. However, the integration of ZCS solid solution with molecular catalyst in CO_2 photoreduction has rarely been studied. Several key scientific issues must be considered in the hybrid system, such as the balance between light absorption and redox ability in ZCS and the electron transfer channel from ZCS to molecular catalyst. What is the predominate factor, or are these factors synergistic? Unfortunately, such questions have rarely been studied in CO_2 photoreduction hitherto. Iron porphyrins-based molecular catalysts have been employed as electro- or photocatalysts for CO_2 reduction to CO due to its high activity and selectivity, earth abundant, and environmentally benign. However, it is noted that majority of the iron porphyrins are

[a] *CAS Key Laboratory of Nanosystem and Hierarchical Fabrication, CAS Center for Excellence in Nanoscience, National Center for Nanoscience and Technology, Beijing 100190, China.*
[b] *Key Laboratory of Photochemical Conversion and Optoelectronic Materials, Technical Institute of Physics and Chemistry, Chinese Academy of Sciences, Beijing 100190, China.*
[c] *University of Chinese Academy of Sciences, Beijing 100049, China.*
E-mail: het@nanoctr.cn; zhangxh@nanoctr.cn; chenyong@mail.ipc.ac.cn
Tel. +86-10-82545655
Electronic Supplementary Information (ESI) available: Chemicals, characterization, EDX mapping, N_2 adsorption-desorption isotherms, CO_2 chemical adsorption isotherms, ICP-MS, Mott-Schotty plots, time dependence of CO evolution amount upon CO_2 photoreduction, UV-vis absorption spectra; SEM, XRD and XPS spectra after CO_2 reduction. See DOI: 10.1039/x0xx00000x

inactive for CO_2 reduction under visible-light irradiation if without efficient photosensitizers.[14,18-20]

Here we have synthesized ZCS solid solutions with well-defined floccule-like morphology comprised of nanoribbons via a facile solvothermal method and fabricated a highly efficient ZCS/tetra(4-carboxyphenyl)porphyrin iron(III) chloride (ZCS/FeTCPP) heterogeneous hybrid catalysts for photoreduction of CO_2 to CO under visible-light irradiation. The composition of the obtained ZCS, i.e., Zn/Cd molar ratio, was modulated by changing the molar ratio of the starting materials. The effects of the changes in local surface environment/atom and band structure of ZCS on the photocatalytic activity of ZCS/FeTCPP hybrid photocatalysts for CO_2 reduction have been studied systematically. Whether or not the ZCS is integrated with FeTCPP, introduction of Zn into CdS can greatly change the activity and selectivity of CO_2 photoreduction. This is mainly because, compared with the pure CdS, the formation of ZCS solid solution can build effective interfacial electron transfer channels from ZCS to FeTCPP.

Experimental

Synthesis of ZCS solid solution and FeTCPP

All the reagents are of analytical grade and used without further purification. ZCS solid solution was synthesized via a solvothermal method using ethylenediamine as solvent and structure-directing agent. In a typical synthesis, 0.5 mmol $Zn(NO_3)_2{\cdot}6H_2O$, 0.5 mmol $Cd(NO_3)_2{\cdot}4H_2O$ and 3 mmol $CS(NH_2)_2$ were dissolved into 30 mL ethylenediamine under constant stirring at room tempreture for 0.5 h. Subsequently, the mixture was transferred into an autoclave and heated at 110 °C for 24 h in a furnace. After cooling to room temperature, the obtained precipitate was separated by centrifugation and washed with ethanol and deionized water alternatively, and dried overnight in vacuum at 65 °C. Finally, the obtained powder was annealed at 400 °C for 2 h under Ar to remove the adsorbed ethylenediamine. A series of ZCS solid solutions with different molar ratio of Zn/Cd were synthesized by changing the molar ratio of the starting material $Zn(NO_3)_2{\cdot}6H_2O$ and $Cd(NO_3)_2{\cdot}4H_2O$ (i.e., 0:1, 0.25:0.75, 0.5:0.5, 0.75:0.25 and 1:0), which were denoted as CdS (ZCS-0), ZCS-1, ZCS-2, ZCS-3 and ZnS (ZCS-4). FeTCPP was synthesized according to the protocol reported previously.[14,21]

Photocatalytic reduction of CO_2

The photocatalytic reduction of CO_2 was carried out in a photoreaction system (Labsolar-IIIAG, Beijing Perfect light Technology Co., Ltd.) saturated with 29 KPa CO_2 using previously reported method.[14] Briefly, 50 mg ZCS solid solution powder with or without 0.3 mg FeTCPP molecular catalyst was suspended under stirring in 100 mL solution of acetonitrile/water/TEOA (3:1:1, v:v:v). The mixed solution was vacuumed and purged with Ar for several times and then was continuously purged high purity CO_2 gas for at least 1.5 h before illumination. The reactor with a constant temperature of 15 °C was illuminated by a 300 W Xe lamp (Microsolar 300, Beijing Perfect light Technology Co., Ltd.) with a 420 nm cut off filter and an IR-cut filter (i.e., 420 nm < λ < 780 nm), the intensity was 260 mW cm^{-2}. The gas products were analyzed by using Agilent 7890A gas chromatography equipped with a hydrogen flame ionized detector (FID) and a thermal conductivity detector (TCD). A series of control experiments (without CO_2 purging, blank solvent without the photocatalysts, without illumination, and only FeTCPP) were performed to ensure that the observed products come solely from photoreduction of CO_2.

Results and discussion

Structure, morphology and optical properties

Fig. 1(a) displays the XRD patterns of the ZCS powder with different molar ratio of Zn/Cd. It is found that the CdS, ZCS-1 and ZCS-2 have similar diffraction patterns to those of hexagonal CdS (JCPDS: 41-1049). From CdS, ZCS-1 to ZCS-2, the diffraction peaks gradually shift to a larger diffraction angle due to smaller ionic radius of Zn^{2+} (0.74 Å) than that of Cd^{2+} (0.94 Å), which is the characteristics of the ZCS solid solution. However, several small individual peaks appearing at around 30.5°, 39.8° and 56.5° that can be attributed to the hexagonal Wurtzite phase ZnS (JCPDS: 36-1450) are present in the sample ZCS-3, implying the occurrence of phase separation with the increased Zn content. The structural homogeneity and the chemical compatibility of the compounds are the prerequisites

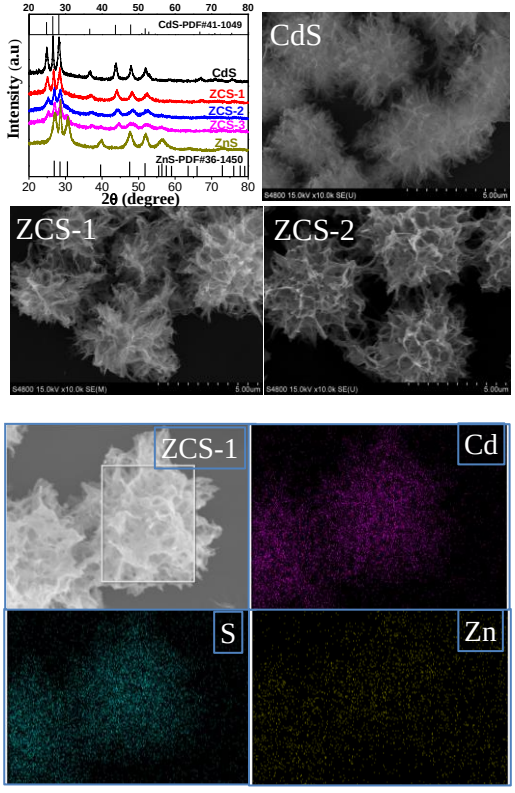

Fig. 1 XRD patterns, SEM images, and EDX mapping (only ZCS-1) of the synthesized ZCS samples.

View Article Online DOI: 10.1039/C8CP02774A

so as to avoid phase separation. As reported previously, it is difficult to directly prepare the ZCS with a large Zn content due to the discrepant physicochemical property between Cd^{2+} and Zn^{2+} ions [17]. In addition, incorporation of Zn into CdS lattice is much more favourable than the reverse process since Zn have a higher mobility than Cd owing to its smaller radius and lighter mass [22]. These may account for the phase separation occurring at high Zn content. Therefore, only CdS, ZCS-1 and ZCS-2 will be discussed in the following sections.

Fig. 1 also shows the FESEM images of CdS, ZCS-1 and ZCS-2. All the synthesized samples exhibit very beautiful floccule-like morphology. Interestingly, when Zn^{2+} ions are incorporated into the lattice of CdS, the floccule-like morphology can be well maintained. The chemical compositions are characterized by using energy-dispersive X-ray spectroscopy (EDX), which are listed in Table S1. However, the Zn/Cd ratios of ZCS-1 and ZCS-2 are not well consistent with that used in the raw materials (Zn^{2+} and Cd^{2+}). The elemental contents for CdS, ZCS-1, and ZCS-2 obtained from EDX analysis are measured to be around $Cd_{0.97}S$, $Zn_{0.14}Cd_{0.84}S$, and $Zn_{0.23}Cd_{0.83}S$, respectively. Additionally, inductively coupled plasma-mass spectrometry (ICP-MS) was further carried out to determine the Zn content. The atomic ratios of Zn to Cd (Zn/Cd) in ZCS-1 and ZCS-2 calculated from ICP-MS are listed in Table S2, which are very similar to those obtained from EDX results. EDX-mapping is then utilized to get further insights into the element spatial distribution. The corresponding elemental mapping images of Zn, Cd and S in ZCS-1 are shown in Fig. 1, while the elemental mapping images of CdS and ZCS-2 are shown in Fig. S1. It clearly reveals the homogeneous distribution of S, Cd and/or Zn in CdS, ZCS-1, and ZCS-2. Moreover, there is no phase separation in ZCS-1 or ZCS-2, confirming the formation of ZCS solid solution.

TEM images further identify the floccule-like morphology of CdS, ZCS-1 and ZCS-2, which is comprised of nanoribbons (Fig. 2). The selected area electron diffraction (SAED) patterns clearly show the polycrystalline nature of the whole flower, of which the diffraction circles are assigned to (100) and (002) crystal facet. The corresponding fast Fourier transform (FFT) patterns indicate the crystalline nature of the individual nanoribbons. In addition, the EDX results from TEM (Table S1) are in good agreement with SEM results.

The typical N_2 adsorption-desorption and CO_2 chemical adsorption isotherms of CdS, ZCS-1 and ZCS-2 are displayed in Fig. S2. BET surface area and CO_2 chemical adsorption capability are listed in Table S1. The BET specific surface area is determined to be 57.99, 72.95 and 95.51 m^2/g for CdS, ZCS-1 and ZCS-2, respectively, which exhibits a trend of gradual increase with increasing Zn content. As for CO_2 chemical adsorption capability, ZCS-1 shows the highest CO_2 adsorption capability (18.06 m^3/g) among the three samples. This is reasonable as the CO_2 adsorption is highly dependent on the surface active sites, not just the BET value measured from the adsorption of N_2 experiment.

The chemical composition and electronic structures of CdS, ZCS-1 and ZCS-2 were analyzed by XPS (Fig. 3a). Two peaks located at 1045.1 and 1021.1 eV with a spin orbit separation of 24.0 eV in Fig. 3(b) are attributed to Zn $2p_{1/2}$ and Zn $2p_{3/2}$ of Zn^{2+}, respectively. The peaks at 411.5 and 404.8 eV in Fig. 3(c) correspond to Cd $3d_{3/2}$ and Cd $3d_{5/2}$, respectively. The splitting energy of 6.7 eV between Cd $3d_{3/2}$ and Cd $3d_{5/2}$ is a typical value for Cd^{2+} in sulfides.[23,24] The peaks at around 162.2 and 161.3 eV in Fig. 3(d) are ascribed to S $2p_{1/2}$ and S $2p_{3/2}$, respectively, which are typical values for S^{2-}. The Zn 2p spectra exhibit almost the same binding energy for ZCS-1 and ZCS-2; while the binding energy for both Cd 3p and S 2p shifts slightly to a higher value from CdS, ZCS-1 to ZCS-2, due to the formation of ZCS solid solutions.

UV-vis absorption spectra of CdS, ZCS-1 and ZCS-2 are shown in Fig. 4(a). The optical absorption edge shows a gradual blue shift with the increased Zn content. The band gap (E_g) has been estimated from these spectra using the Kubelka-Munk method (inset of Fig. 4(a)). The E_g value of CdS, ZCS-1 and ZCS-2 is calculated to be 2.42, 2.46, and 2.51 eV, respectively. So the introduction of Zn into CdS increases the E_g slightly, indicating that the E_g of ZCS solid solutions can be tuned via tailoring the Zn/Cd ratio. XPS valence spectroscopy (Fig. 4b) was measured to estimate the valence band (E_{VB}), which is determined to be about 1.18, 1.20 and 1.24 V (vs NHE)

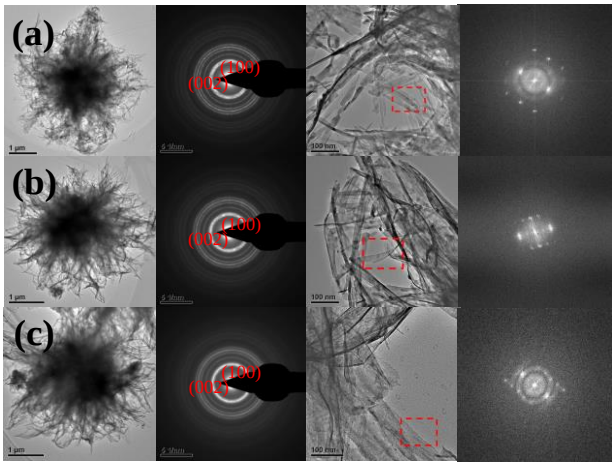

Fig. 2 TEM image, SAED pattern, and live FFT of (a) CdS, (b) ZCS-1, and (c) ZCS-2.

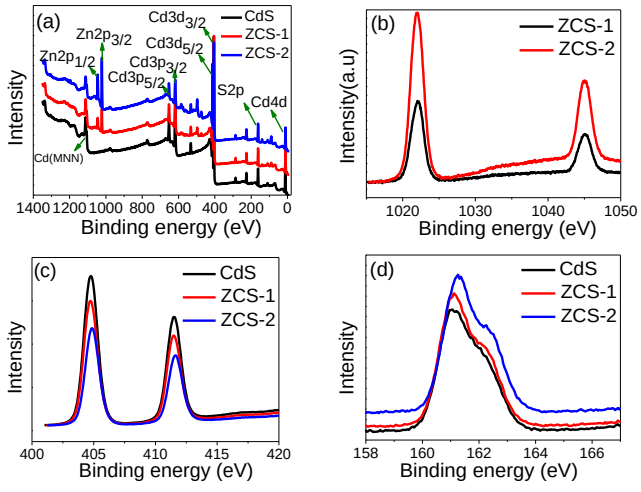

Fig. 3 (a) XPS survey spectra of CdS, ZCS-1 and ZCS-2, high-resolution XPS spectra of (b) Zn 2p, (c) Cd 3d, and (d) S 2p for CdS, ZCS-1 and ZCS-2.

View Article Online
DOI: 10.1039/C8CP02774A

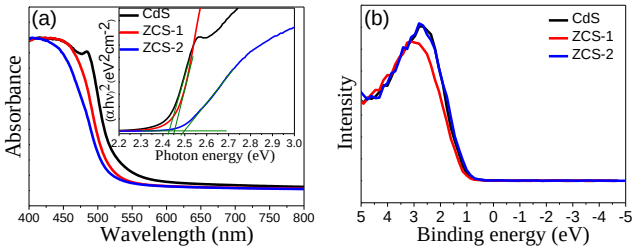

Fig.4 (a) UV-vis absorption (inset, Tauc plot) and (b) XPS valence band of CdS, ZCS-1 and ZCS-2.

for CdS, ZCS-1 and ZCS-2, respectively. Combining with E_g obtained from Fig. 4(a), the conduction band (E_{CB}) value for CdS, ZCS-1 and ZCS-2 is calculated to be −1.24, −1.26 and −1.27 V (vs NHE), respectively. The band structure of the obtained ZCS solid solution changes obviously with the introduction of Zn. The CB value for all the CdS, ZCS-1 and ZCS-2 is negative than the redox potential of FeTCPP (−1.02 V, vs NHE), indicating that the electrons transfer from the CB of CdS and ZCS to FeTCPP is thermodynamicly feasible.[14]

The Mott-Schottky plots of CdS, ZCS-1, and ZCS-2 (Fig. S3) are further used to determine the flatband potential (E_{FB}), which is the key factor that determines the charge transfer direction, which is −1.09 V, −1.10 V, and −1.16 V (vs. NHE) for CdS, ZCS-1 and ZCS-2, respectively. So all the E_{FB} values are negative than the reduction potential of FeTCPP ($E_{Fe}^{I/0}$, −1.02 V vs NHE), implying that the electron transfer from both CdS and ZCS to FeTCPP is thermodynamicly feasible. Considering the E_{CB} of n-type semiconductors is more negative than E_{FB}, the electron can indeed transfer from both CdS and ZCS to FeTCPP, consistent with the above results.

PL and ESR characteristics

The amount of photogenerated electrons are not only related with the light absorption ability of semiconductor materials, but also highly dependent on the separation of charge carriers, which is usually studied by PL and time-resolved PL measurements. Fig. 5(a) shows the PL spectra of CdS, ZCS-1 and ZCS-2. CdS exhibits a strong PL signal at around 540 nm when excited by 350 nm. It is found that ZCS-1 ($Zn_{0.14}Cd_{0.84}S$) has weaker PL signal than CdS, while ZCS-2 ($Zn_{0.23}Cd_{0.83}S$) has a slightly stronger PL signal than CdS, indicating that appropriate amount of Zn can reduce the electron-hole combination, i.e. increase the charge seperation. The broad asymmetric tail in all of the luminescence peaks can be attributed to the large amount of the defect/surface states formed during synthesis.[25] Since the ionic radius of Zn^{2+} and Cd^{2+} has approximately 10% difference, compared with the PL spectrum of CdS, the slighly red-shifted PL spectra of ZCS-1 and ZCS-2 may be caused by higher amount of the defect/surface states due to the release of lattice strain in the crystals upon Zn incorporation.[22]

Fig. 5(b) shows the time-resolved PL decay curves of the as-synthesized ZCS samples, the corresponding fitted fluorescence lifetime and calculated average lifetime are listed in Table 1. All of the samples show the tri-exponential decay characteristics, corresponding to the three different processes that contribute to the lifetime, non-radiative process (τ_1), radiative process (τ_2) related to the recombination of photogenerated electrons and holes, and energy transfer process (τ_3).[26,27] There are two different energy transfermechanisms, fluorescence resonance energy transfer (FRET) and radiation-reabsorption. FRET is a distance-dependent interaction between the electronic excited states of two molecules, in which excitation is transferred from the donor molecule to acceptor molecule without photon emission. Here the τ_3 is mainly associated with the radiation-reabsorption process, as no photon emission and reabsorption is involved in FRET. The average lifetime (τ) is calculated by the equation of $\tau=f_1\tau_1+f_2\tau_2+f_3\tau_3$, where f is the relative fractional contribution.[28] ZCS-2 exhibits a very similar τ to CdS, while ZCS-1 has the slowest decay kinetics and shows the longest τ among CdS, ZCS-1 and ZCS-2, implying the highest charge separation efficiency in ZCS-1 (i.e., efficient charge transfer from ZCS-1 to FeTCPP, as discussed later).

Table 1. Fluorescence lifetime of CdS, ZCS-1 and ZCS-2, derived from time-resolved PL decay curves.

Sample	τ_1 / ns (rel. %)	τ_2 / ns (rel. %)	τ_3 / ns (rel. %)	τ / ns
CdS	1.04 (38.07%)	6.05 (31.76%)	100.90 (30.17%)	32.77
ZCS-1	0.90 (33.21%)	5.82 (28.88%)	126.48 (37.92%)	49.94
ZCS-2	0.99 (38.37%)	6.33 (32.98%)	107.52 (28.65%)	33.27

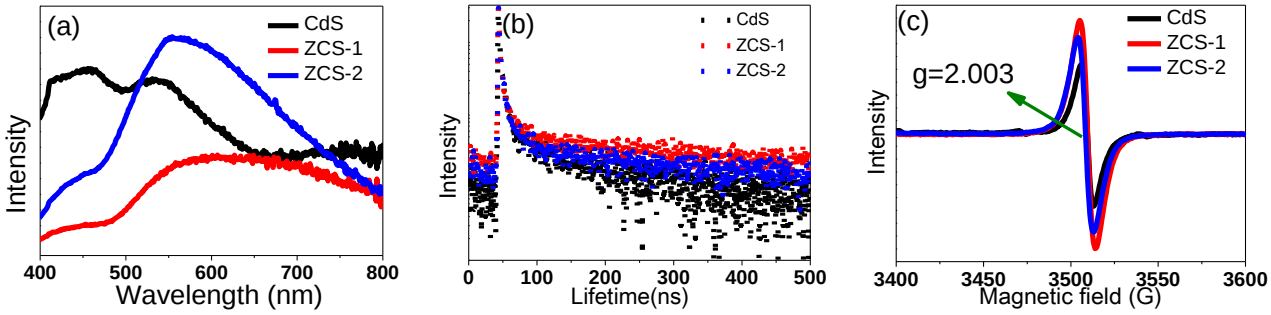

Fig. 5 (a) PL spectra excited by 350 nm, (b) time-resolved PL decay curves at 540 nm, and (c) ESR spectra of CdS, ZCS-1 and ZCS-2.

View Article Online
DOI: 10.1039/C8CP02774A

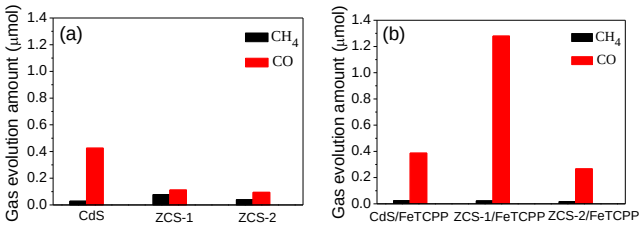

Fig.6 CO_2 photoreduction results over different catalysts (a) without and (b) with FeTCPP (0.3 mg) in CH_3CN:H_2O:TEOA (3:1:1, 100 mL) mixed solution under visible-light illumination (420 nm < λ < 780 nm), light intensity = 260 mW cm^{-2}.

It is noted that the charge separation in a semiconductor can be related to the defects. Therefore, ESR characterization was further performed. As shown in Fig. 5(c), the typical sulfur vacancy signals at g = 2.003 was observed.[29] ZCS-1 shows the highest ESR signal, followed by ZCS-2 and CdS. Thus, the introduction of Zn into CdS can facilitate the formation of sulfur vacancy, which can affect the catalytic efficiency of ZCS/FeTCPP hybrid catalysts via two approaches, i.e., charge separation in ZCS and interaction mode between ZCS and FeTCPP. The sulfur vacancy can serve as the center for electron trapping and active sites for CO_2 adsorption. In this sense, one can also say the sulfur vacancy can facilitate the separation of charge carriers. The more sulfur vacancy, the higher charge separation efficiency is. This also explains why the CO_2 chemical adsorption follows the order of CdS < ZCS-2 < ZCS-1(Fig. S2(b)). Furthermore, sulfur vacancy can also enhance the interaction between the ZCS and FeTCPP, which can promote the interfacial electron transfer between the ZCS and FeTCPP.

Photoreduction of CO_2 over ZCS and ZCS/FeTCPP catalysts

Fig. 6(a) and 6(b) show the respective results of CO_2 photoreduction over ZCS and ZCS/FeTCPP catalysts under visible-light illumination (420 nm ≤ λ ≤ 780 nm). The major products are CH_4 and CO, with very little amount of H_2 due to the competitive reaction of water splitting. No any other gas or liquid products were observed within 4-h irradiation. The accurate amount of the produced H_2 cannot be calculated due to the detection limit of the GC instrument. Without the FeTCPP, the amount of produced CH_4 and CO from CO_2 reduction over CdS after 4-h illumination is 0.028 and 0.43 μmol, respectively. When the ZCS-1 and ZCS-2 were used, the amount of CH_4 increase obviously (0.078 and 0.039 μmol for ZCS-1 and ZCS-2, respectively), while the amount of CO decreases greatly (0.11 and 0.095 μmol for ZCS-1 and ZCS-2, respectively) (Fig. 6a). These indicate that the introduction of Zn into CdS can significantly affect the product selectivity of CO_2 reduction and facilitate the formation of CH_4, which may be due to the different adsorption ability of the intermediates and products on ZCS solid solutions. Moreover, it is noted that the amount of both CH_4 and CO for ZCS-2 is less than that for ZCS-1. Considering ZCS-2 has a larger BET value, this is possibly because the ZCS-2 exhibits inferior CO_2 adsorption capability and charge separation efficiency to the ZCS-1, as discussed above. Here the influence of band structure (mainly including E_g and E_{CB}; the former can affect the light absorption and the latter can have an impact on the reduction power) is not considered, as the difference among the three samples is not large enough to cause an obvious change.

Compared with the case using pure CdS, the amount of both CH_4 and CO using CdS/FeTCPP hybrid catalysts decreases slightly (0.024 and 0.39 μmol, respectively), indicating that the electrons in the CB of CdS cannot efficiently transfer to FeTCPP. This maybe because the interaction between CdS and FeTCPP is not strong enough and/or the FeTCPP may hinder light harvesting of CdS since FeTCPP has a strong Soret-band absorption at 428 nm but inactive under visible-light irradiation without the light-harvesting absorber.[30,31] Interestingly, compared with pure ZCS-1 (0.078 and 0.11 μmol for CH_4 and CO, respectively), the amount of CO using ZCS-1/FeTCPP hybrid catalysts (1.28 μmol) increases greatly, while the amount of CH_4 (0.023 μmol) decreases obviously. The TON value of the ZCS-1/FeTCPP hybrid catalyst is calculated to be about 9.2 after 12-h reduction based on the FeTCPP amount (Fig. S4). If further increasing the Zn amount (such as ZCS-2), the CO yield for ZCS-2/FeTCPP (0.27 μmol) is much less than that of ZCS-1/FeTCPP, while still noticeably higher than that of pure ZCS-2 (0.095 μmol). However, the CH_4 yield for ZCS-2/FeTCPP (0.017 μmol) is less than that of both ZCS-1/FeTCPP (0.023 μmol) and pure ZCS-2 (0.039 μmol). Nevertheless, considering the electrons involved in the CO_2 reduction for the observed products, the integration with FeTCPP (0.844 and 2.744 μmol for ZCS-1 and ZCS-1/FeTCPP, respectively; 0.502 and 0.676 μmol for ZCS-2 and ZCS-2/FeTCPP, respectively) can improve the production yield, not just greatly change the reduction selectivity. In addition, it is found that the ZCS solid solution based hybrid catalyst exhibits higher stability than the CdS based hybrid catalyst (Fig. S5). Moreover, the ZCS-1/FeTCPP catalyst shows linear increase of the CO yield over upon CO_2 reduction under visible-light illumination even for 12 h (Fig. S5). So the ZCS-1/FeTCPP is quite stable, which is well consistent with the previous work.[32,33] Based on the results of XRD, XPS, and SEM images of the CdS, ZCS-1 and ZCS-2 after CO2 photoreduction (Fig. S6 and S7), it is concluded that the deactivation of CdS/FeTCPP may originate from the instability of CdS, rather than the decomposition of FeTCPP.

Scheme 1 shows the schematic diagram of CO_2 photoreduction over the ZCS/FeTCPP hybrid catalyst, which consists of the following processes, generation of photoelectrons in ZCS upon visible-light illumination, followed by the electrons transfer from ZCS to FeTCPP, and then CO_2 reduction on FeTCPP. Meanwhile, the holes left in VB of ZCS are consumed by sacrificial agent TEOA. Obviously, the construction of an efficient ZCS/FeTCPP hybrid for CO_2 photoreduction strongly depends on the charge generation/separation in ZCS and the effective electron transfer from ZCS to FeTCPP. However, it seems that the photogenerated electrons cannot efficiently transfer from CdS to FeTCPP even in the case that the CB potential of CdS (–1.24 V) is more negative than the redox potential of FeTCPP (–1.02 V), as mentioned above.

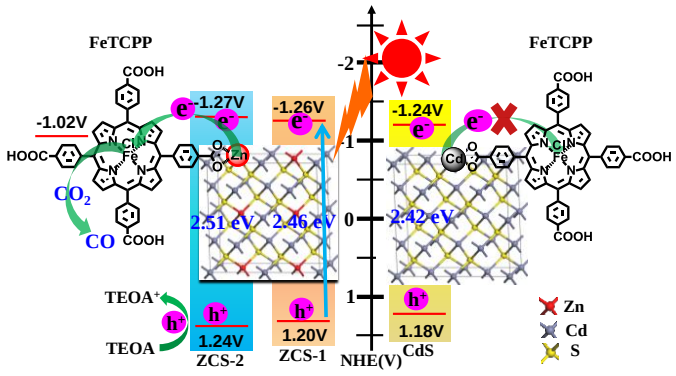

Scheme 1. Schematic diagram of CO_2 photoreduction over ZCS/FeTCPP hybrid catalyst.

While for the ZCS, introduction of Zn may affect the interaction between the FeTCPP and ZCS due to the changes in surface atoms of CdS and/or the differences in the coordination ability of carboxyl groups with Zn^{2+} and Cd^{2+}, which can build an effective electron transfer channel from ZCS solid solutions to FeTCPP. It is noted that the ZCS contains more sulfur vacancy than CdS, which can facilitate the interaction between the ZCS and FeTCPP. Moreover, the binding energy for both Cd 3p and S 2p shifts slightly to a higher value upon the introduction of Zn into CdS (Fig. 3), implying that the electronic density decreases upon Zn introduction. This is in favor of the modification of FeTCPP onto the semiconductor, as the molecular catalyst contains COO^- end group in basic solution. In addition, it is noted thatthe ZCS-1/FeTCPP shows much higher photoreduction activity than ZCS-2/FeTCPP. A total amount of 1.28 μmol of CO with selectivity of 93% was achieved using 50 mg of ZCS-1 integrated with 0.3 mg of FeTCPP after 4 h irradiation under visible-light irradiation. This may be mainly because the ZCS-1 exhibits higher charge separation efficiency and electron transfer efficiency than ZCS-2, as well as more sulfur vacancy. Again, here the influence of band structure is ignored, as discussed above.

Conclusions

In conclusion, ZCS solid solutions with well-defined floccule-like morphology comprised of nanoribbons have been successfully synthesized. The introduction of appropriate amount of Zn into CdS can change the charge separation efficiency and the interaction mode with FeTCPP. Most important, the presence of Zn can also strengthen the coupling of CdS with FeTCPP, which can build effective interfacial channels for electron transfer from ZCS to FeTCPP and, thereby, greatly increase the photocatalytic activity of ZCS/FeTCPP hybrid catalysts for CO_2 reduction. ZCS-1/FeTCPP ($Zn_{0.14}Cd_{0.84}S$/FeTCPP) exhibits the highest photocatalytic activity for CO_2 reduction to CO under visible-light irradiation by virtue of the efficient charge separation, effective electron transfer and more sulfur vacancy. About 1.28 μmol of CO with selectivity of 93% is achieved over ZCS-1/FeTCPP after 4 h under visible-light irradiation. We envision that this work may afford a better understanding of CO_2 photoreduction over the solid solution/molecular catalyst hybrid systems, and provide a feasible approach to fabricate highly efficient heterogeneous photocatalysts for CO_2 reduction.

View Article Online
DOI: 10.1039/C8CP02774A

Conflicts of interest

There are no conflicts to declare.

Acknowledgements

This work was supported by the National Natural Science Foundation of China (21673052), the Ministry of Science and Technology of China (2015DFG62610), and The Belt and Road Initiative by Chinese Academy of Sciences.

Notes and references

1 J. L. White, M. F. Baruch, J. E. Pander III, Y. Hu, I. C. Fortmeyer, J. Eujin Park, T. Zhang, K. Liao, J. Gu, Y. Yan, T. W. Shaw, E. Abelev and A. B. Bocarsly, *Chem. Rev.*, 2015, **115**, 12888–12935.
2 X. X. Chang, T. Wang and J. L. Gong, *Energy Environ. Sci.*, 2016, **9**, 2177–2196.
3 Y. Gao, L. Ye, S. Y. Cao, H. Chen, Y. N. Yao, J. Jiang and L. C. Sun, *ACS Sustainable Chem. Eng.*, 2018, **6**, 781–786.
4 K. Teramura and T. Tanaka, *Phys. Chem. Chem. Phys.*, 2018, **20**, 8423-8431.
5 L. Q. Ye, J. Mao, T. Y. Peng, L. Zan and Y. X. Zhang, *Phys. Chem. Chem. Phys.*, 2014, **16**, 15675-15680.
6 Y. Chen, G. Jia, Y. Hu, G. Fan, Y. H. Tsang, Z. Li and Z. Zou, *Sustainable Energy Fuels*, 2017, **1**, 1875–1898.
7 A. J. Morris, G. J. Meyer and E. Fujita, *Acc. Chem. Res.*, 2009, **42**, 1983–1994.
8 H. Takeda, C. Cometto, O. Ishitani and M. Robert, *ACS Catal.*, 2017, **7**, 70–88.
9 K. Li, B. Peng and T. Peng, ACS Catal., 2016, **6**, 7485–7527.
10 X. Liu, S. Inagaki and J. L. Gong, *Angew. Chem. Int. Ed.*, 2016, **55**, 14924–14950.
11 F. Wen and C. Li, Acc. Chem. Res., 2013, **46**, 2355–2364.
12 K. Muraoka, H. Kumagai, M. Eguchi, O. Ishitani and K. Maeda, *Chem. Commun.*, 2016, **52**, 7886–7889.
13 G. X. Zhao, H. Pang, G. G Liu, P. Li, H. M. Liu, H. B. Zhang, L. Shi and J. H. Ye, *Appl. Catal. B: Environ.*, 2017, **200**, 141–149.
14 L. Lin, C. C. Hou, X. H. Zhang, Y. J. Wang, Y. Chen and T. He, *Appl. Catal. B*, 2018, **221**, 312–319.
15 W. Li, D. Li, W. Zhang, Y. Hu, Y. He and X. Fu, *J. Phys. Chem. C*, 2010, **114**, 2154–2159.
16 Q. Li, H. Meng, P. Zhou, Y. Zheng, J. Wang, J. Yu and J. Gong, *ACS Catal.*, 2013, **3**, 882–889.
17 Z. Han, G. Chen, C. Li, Y. Yu and Y. Zhou, *J. Mater. Chem. A*, 2015, **3**, 1696–1702.
18 C. Costentin, S. Drouet, M. Robert and J. M. Saveant, *Science*, 2012, **338**, 90–94.
19 J. Bonin, M. Robert and M. Routier, *J. Am. Chem. Soc.*, 2014, **136**, 16768–16771.
20 S. Lian, M. S. Kodaimati, D. S. Dolzhnikov, R. Calzada and E. A. Weiss, *J. Am. Chem. Soc.*, 2017, **139**, 8931–8938.
21 G. Granados-Oliveros, E. A. Páez-Mozo, F. M. Ortega, C. Ferronato and J. M. Chovelon, *Appl. Catal. B*, 2009, **89**, 448–454.
22 S. Biswas, S. Kar, S. Santra, Y. Jompol, M. Arif and S. I. Khondaker, *J. Phys. Chem. C*, 2009, **113**, 3617–3624.

View Article Online
DOI: 10.1039/C8CP02774A

23 H. Zhao, Y. M. Dong, P. P. Jiang, G. L. Wang, H. Y. Miao, R. X. Wu, L. G. Kong, J. J. Zhang and C. Zhang, *ACS Sustainable Chem. Eng.*, 2015, **3**, 969−977.
24 X. Y. Zhang, Z. Zhao, W. Zhang, G. Q. Zhang, D. Qu, X. Miao, S. R. Sun and Z. C. Sun, *Small*, 2016, **12**, 793–801.
25 S. Kar, B. Satpati, P. V. Satyam and S. Chaudhuri, *J. Phys. Chem. B*, 2005, **109**, 19134–19138.
26 H. B. Zhang, J. Wei, J. C. Dong, G. G. Liu, L. Shi, P. F. An, G. X. Zhao, J. T. Kong, X. J. Wang, X. G. Meng, J. Zhang and J. H. Ye, *Angew. Chem. Int. Ed.*, 2016, **55**, 14522–14526.
27 X. Y. Guo, W. Y. Song, C. F. Chen, W. H. Di and W. P. Qin, *Phys. Chem. Chem. Phys*., 2013, **15**, 14681–14688.
28 J. R. Lakowicz, Principles of Fluorescence Spectroscopy Principles of Fluorescence Spectroscopy, Springer, Heidelberg, 2007.
29 Z. Fang, S. Weng, X. Ye, W. Feng, Z. Zheng, M. Lu, S. Lin, X. Fu and P. Liu, *ACS Appl. Mater. Interfaces*, 2015, **7**, 13915–13924.
30 J. Bonin, M. Chaussemier, M. Robert and M. Routier, *ChemCatChem*, 2014, **6**, 3200–3207.
31 J. Grodkowski, D. Behar and P. Neta, *J. Phys. Chem. A*, 1997, **101**, 248–254.
32 F. Yang, N. N. Yan, S. Huang, Q. Sun, L. Z. Zhang and Y. Yu, *J. Phys. Chem. C*, 2012, **116**, 9078–9084.
33 S. L. Xie, X. H. Lu, T. Zhai, J. Y. Gan, W. Li, M. Xu, M. H. Yu, Y. M. Zhang and Y. X. Tong, *Langmuir*, 2012, **28**, 10558–10564.

View Article Online
DOI: 10.1039/C8CP02774A

Visible-light driven CO_2 photoreduction over $Zn_xCd_{1-x}S$ solid solution coupling with tetra(4-carboxyphenyl)porphyrin iron(III) chloride

Pan Li,[a,c] Xuehua Zhang,[a,*] Chunchao Hou,[b] Lin Lin,[a] Yong Chen,[b,c,*] Tao He[a,c,*]

[a] CAS Key Laboratory of Nanosystem and Hierarchical Fabrication, CAS Center for Excellence in Nanoscience, National Center for Nanoscience and Technology, Beijing 100190, China.

[b] Key Laboratory of Photochemical Conversion and Optoelectronic Materials, Technical Institute of Physics and Chemistry, Chinese Academy of Sciences, Beijing 100190, China.

[c] University of Chinese Academy of Sciences, Beijing 100049, China

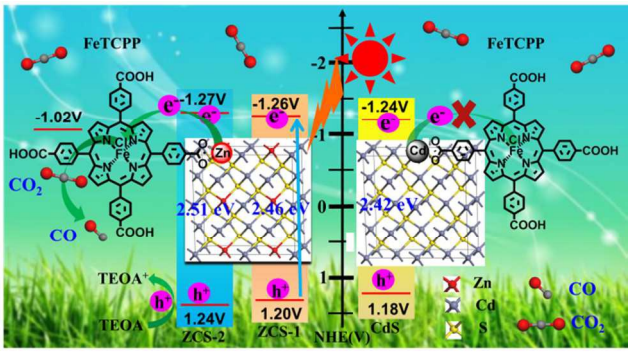

Photocatalytic reduction of CO_2 into solar fuels is a promising approach to supply sustainable energy and efficiently use CO_2 as a resource.